α-Ni(OH)2 thin films fabricated by liquid phase deposition method

Deki, Shigehito

Hosokawa, Akinobu

Beleke, Alexis Bienvenu

Mizuhata, Minoru

α-Ni(OH)$_2$ thin films fabricated by liquid phase deposition method

Shigehito Deki*, Akinobu Hosokawa, Alexis Bienvenu Béléké, and Minoru Mizuhata

Department of Chemical Science and Engineering,

Graduate School of Engineering, Kobe University,

1-1 Rokko, Nada, Kobe 657-8501, Japan

Abstracts:

α-Ni(OH)$_2$ thin films have been synthesized on various substrates by liquid phase deposition method. The deposited films were characterized by X-ray diffraction, X-ray photoelectron spectroscopy and scanning electron microscope (SEM). The addition of boric acid (H$_3$BO$_3$) as fluoride scavenger to the treatment solution destabilized the [NiF$_x^{(x-2n)-}$] metal-fluoro complex bonds and forced the oxide precipitation, resulting in the formation of α-Ni(OH)$_2$. The obtained thin films exhibited transparency and interference color. SEM images showed that the films consisted of interconnected thread-like fibers with a width of ca. 50 nm. The deposition process and morphology of fibrous particles showed strong dependence to the initial concentrations of H$_3$BO$_3$ solution and temperature. Transparency and interference color were related to the film thickness, which can be controlled by the concentration of Ni metal-fluoro complex and the reaction time. Calcination at 500°C led to the formation of NiO particles. For comparison purpose, β-Ni(OH)$_2$ thin films prepared by "direct deposition" method which consists of simple heterogeneous nucleation in an aqueous solution without adding boric acid is reported.

Keywords: nickel hydroxide, liquid phase deposition, direct deposition, thin films, morphology

1. Introduction

Nickel hydroxide $Ni(OH)_2$ has received increasing attention in the recent years not only due to its application as an active material in nickel-based secondary batteries owing its good cycle ability, high specific power and specific energy, but also because it serves as starting material for nickel oxide which has many technological applications in ceramic and glass industry [1-4]. Crystallographic studies established that nickel hydroxide has a hexagonal layered structure with two polymorphs designated as α-$Ni(OH)_2$ and β-$Ni(OH)_2$, respectively. The α-phase displays a more disorderly and larger interlamellar spacing (depending on the type and extend of intercalated species) which contains anions such as nitrate, carbonate, sulfate and water molecules. The β-phase possesses a brucite-like structure, well oriented $Ni(OH)_2$ layers and perfectly stacked along the c axis with an interlamellar distance of 4.6 Å and does not contain any intercalated species [5].

In most cases, the β-phase of $Ni(OH)_2$ is utilized as an active material of nickel-based positive electrodes whilst it is generally recognized that the α-phase provides a higher electrochemical reactivity than the β-phase, presumably due to the higher mobility of OH and H_2O within the largely separated nickel hydroxide layers [6]. However, the α-phase is known to be the metastable one and difficult to synthesize because it rapidly changes to β-phase during synthesis, or in the presence of strong alkaline solution as in the case of battery electrolyte [5].
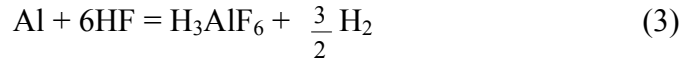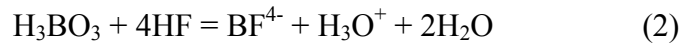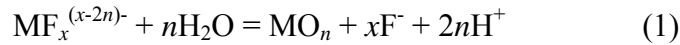
Several methods of synthesis of $Ni(OH)_2$ have been proposed in the literature, and most of them deal with the β-type. Among these methods, chemical precipitations are the most used ones [7, 8]. Although these methods are simple because they basically involve the mixing of nickel salt solutions and bases, reproducibility is seldom warranted due to the very large supersaturations attained, especially when α-$Ni(OH)_2$ is the desired product [9]. In some cases, the procedure leads to a mixture of α and β hydroxides if the precipitation

reaction is not quenched rapidly [10]. Since it is well established that the overall performance of nickel cathodes depends on the microstructure, textural characteristics, and the crystallite size of the active material [11], a simple and reliable synthesis procedure of α-Ni(OH)$_2$ becomes a matter of importance.

Akinc et al. succeeded in the synthesis of the turbostatic α-phase nickel hydroxide powders by urea decomposition. However, their technique necessitated an addition of dispersant to increase the specific surface area [12]. Jeevanandam and co-workers synthesized fibrous nanosized α-Ni(OH)$_2$ with an interlayer spacing of 7.2 Å by sonochemical method [13]. The authors got scaly particles with length of ca. 200 nm and a width of ca. 15 nm. Xia et al. obtained spherical nanocrystallines α-Ni(OH)$_2$ with a particle size of about 20 nm by ultrasonic precipitation [14]. Recently, Li-Xia et al. used hydrothermal technique in mixed solvents of water and alcohol to synthesize both α and β phases of nanosheets and nanoflowers nickel hydroxides [15]. The obtained product was α-Ni(OH)$_2$ which could be transformed to β-Ni(OH)$_2$ by adjusting hydrothermal time. These outstanding references point out the degree of challenge required for a simple and reliable technique for the synthesis of α-Ni(OH)$_2$.

Herein we report a facile strategy to synthesize a stable phase of α-nickel hydroxide thin films using the liquid phase deposition (LPD) method. The concept was developed by Kawahara's group for the synthesis of silica (SiO$_2$) thin film [16, 17], and we have been reporting various types of metal oxide and alloy thin films prepared by LPD for the past two decades [18-24]. Nowadays, many research groups around the world are using this process as method of preparation of solid oxide thin films, due certainly to number of advantages over other methods of synthesis [25, 26].

The main reactions in LPD process can be expressed as follows:

$$MF_x^{(x-2n)-} + nH_2O = MO_n + xF^- + 2nH^+ \qquad (1)$$

$$H_3BO_3 + 4HF = BF^{4-} + H_3O^+ + 2H_2O \qquad (2)$$

$$Al + 6HF = H_3AlF_6 + \frac{3}{2}H_2 \qquad (3)$$

Addition of boric acid is the most common technique. The role of boric acid is not only to serve as fluoride scavenger, but it also shifts reaction (1) to the right side by producing water. Once the oxide's solubility limit is reached, homogeneous nucleation occur, and thin films are formed by crystal and random structured oxide layer from the substrate and the oxide layer grows onto the substrate.

In the early work by Nagayama et al.[16], it was clearly demonstrated that thin films fabricated by LPD method have a dense structure and a superior chemical stability that warranted reproducibility, good processability, and durability under continuous use. Silica film deposited on glass substrate (which is used for the transparent electrode of flat panel displays such as liquid crystal display and electroluminescent display) exhibited a more orderly silica network and low etch rate than films prepared by other methods such as vacuum evaporation and dipping method. It was also shown that the deposition rate is influenced by the degree of supersaturation which is related to the temperature of the solution and the quantity of added boric acid. Furthermore, in our previous report on the growth of iron oxyhydroxide (β-FeOOH) thin film deposited on Au substrate, high resolution transmission electron microscopy image near the film/substrate interface has indicated that the films showed strong adherence to the substrate with epitaxial growing of oxide film even at the solid/liquid interface [22]. Therefore, it is believed that for LPD Ni(OH)$_2$ film, charge transfer will occur at the current collector/active material interface of the electrode.

In this study, we describe a very simple route for the preparation of stable α-Ni(OH)$_2$ thin films. The surface morphology of the films and the deposition process are controlled by

the reaction conditions. Furthermore, nickel oxide thin film could be obtained by calcination of the prepared nickel hydroxide. The obtained samples were characterized by X-ray diffraction (XRD), X-ray photoelectron spectroscopy (XPS) and scanning electron microscope (SEM). β-Ni(OH)$_2$ thin films prepared by "direct deposition" (DD) method are briefly analyzed for comparison purpose.

2. Experimental details

2.1 Sample preparation

The Ni parent solution was prepared as follows: 120 g of Ni(NO$_3$)$_2$·6H$_2$O (Nacalai Tesque Inc.) were dissolved into 800 ml of ion exchange water and, while keeping under stirring, ca.50 ml of 33 vol % of aqueous NH$_3$ (Nacalai Tesque Inc.) was drop-wisely added until pH reached 7.5. The collected precipitate was repeatedly washed with ion exchange water and dried at ambient temperature. It was then agitated into 750 ml of 0.66 mol dm^{-3} NH$_4$F (Nacalai Tesque Inc.) for 48 h at ambient temperature, and filtered to give Ni parent solution. Later, the Ni parent solution was mixed with H$_3$BO$_3$ (Nacalai Tesque Inc.) and ion exchange water in a plastic bottle at various concentrations to serve as treatment solution.

Depending on the experiment target, Soda-lime glass (Matsunami Glass Industry Inc.), alumina (Al$_2$O$_3$) (Showa Electric Co.) or single-crystal silicon (Si) wafer (Mitsubishi Electric Corporation Inc.) were used as substrates. Soda-lime glass or Al$_2$O$_3$ substrates were degreased and washed ultrasonically with water prior to use whereas Si wafer substrates were merely immersed into diluted fluoric acid (HF) solution for 30 sec and washed with water. These substrates were then immersed in the treatment solution and suspended therein vertically. Reactions were carried out at 40°C at various periods of time up to 48 hours. The substrates were then removed from the solution, washed and dried at ambient temperature for 24 h. For the achievement of NiO, the deposited films were heat treated in an air flow for

1 h at different temperatures ranging from 500 to 1000°C.

2.2   Characterization of deposited films

The crystalline structures were investigated using X-ray diffractometer (Rigaku RINT-TTR/S2) equipped with a scintillation detector, and a rotating Cu anode operating radiation at 50 kV and 300 mA. Using parallel beam optics formed by a multilayered mirror (Rigaku, Cross Beam Optics attachment), asymmetric 2θ scans with a fixed small incident angle were carried out. In comparison with Bragg-Brentano geometry, the 2θ scans allowed to sufficiently increase the intensity of diffracted peaks that belongs to the surface of thin films. A scan rate of 4 ^{o} per minute was applied within the range of 5 − 70° and, the X-ray incident angle was set to 1°.

Chemical states of Ni and O comprising into the films were analyzed with XPS (JEOL JPS-9010MC). Measurements were conducted using AlKα as the X-ray source (1486.6 eV) at power of 300 W (i.e. 10 kV potential and 30 mA emission current). Samples were mounted on carbon adhesive sheet, stored into the sample chamber for ca.12 h under vacuum for ageing purpose and removing humidity. Therein they were maintained at ambient temperature and a pressure of 100 mPa throughout the experiment. Calibration for spectra was performed by taking the C 1s electron peak (E_b = 284.6 eV) as internal reference.

The surface morphologies of the films were observed by field emission scanning electron microscope (JEOL JEM-6335F). An acceleration voltage of 15 kV was applied. In order to prevent the surface of samples from electron charging up, carbon was coated on the samples using carbon coater (40FM; Meiwa Shoji Co. Ltd.).

The amount of Ni contained in the deposited film or reaction solution was measured by inductively coupled plasma atomic emission spectrometry (HORIBA Ltd., ULTIMA 2000). The deposited films on a substrate were dissolved into 20 ml of 0.17 mol dm^{-3} HNO$_3$. Standard nickel solution with a concentration of 1000 ppm was used as reference sample. The main operating conditions during the measurements are summarized in Table 1. The optical transmission and scattering measurements of reaction solution were performed using UV-Vis Spectrophotometer (JASCO V 7200). Measurements were conducted within the range from 350 to 800 nm.

2.3 Preparation of β-Ni(OH)$_2$ by direct deposition with hydrolysis reaction

For comparison purpose, the β-phase obtained by a method close but fundamentally different from LPD that we call "direct deposition" is also reported. The synthesis procedures employed for the obtaining β-Ni(OH)$_2$ are strictly the same as those for α-Ni(OH)$_2$, except that boric acid was not added. This means that the same Ni parent solution (used for the preparation α-Ni(OH)$_2$) with an initial concentration of 30 mmol dm^{-3} was simply mixed with ion exchange water and served has treatment solution.

3 Results and discussion

3.1 Analysis of the deposited films

Fig.1(a) shows XRD patterns of the deposited nickel hydroxide thin films prepared by LPD method. The *d* values are 6.99, 3.52, 2.67 and 1.54 Å, and could be assigned to (003), (006), (101), and (110) planes, respectively, indicating the formation of an α-phase. Except for the reflection at 6.99 Å which is lower, the *d* values of the other three reflections are consistent with those reported by Jeevanandam et al. [13]. The existence of the interplanar spacing at 6.99 Å is characteristics of an imperfect crystalline organization of α-nickel

hydroxide [5]. Furthermore, the asymmetric nature of the reflection at 2.66 Å indicates the formation of a turbostatic phase observed in most of the α-type hydroxides [13].

The interlayer spacing of 6.99 Å found in this work is somewhat lower than those reported in the literature for non-dehydrated α-nickel hydroxides. Dennstedt and Loser [27] and Le Bihan and Figlarz [28] studied the thermal decomposition of nickel hydroxides and observed a lowering of the interplanar distance from 8.5 to 7 Å between two $Ni(OH)_2$ only after a thermal treatment at 150^oC. The authors found that such variation was fully reversible by rehydration and, their thermoanalysis suggested that the stacked structure less than 7 Å would correspond to the presence of monomolecular intersheet water layers.   A decrease in the intersheet distance from 8.1 to 6.9 Å was also observed after dehydration of the so-called αC (a term used by the authors to identify α-nickel hydroxides containing an equal amount of carbonate and nitrate anions) by Portemer et al.[29]. Thermal gravimetric analysis (TGA) by Faure et al. [8] showed that only partially dehydrated phase displays an intersheet distance close to 7.2 Å. Otherwise, the d value generally obtained falls in the range from 7.2 to 9.0 Å, depending basically on the amount and size of corresponding anions and water molecules intercalated and/or adsorbed [6-15, 27-29]. Synthesis by precipitation method generally results in the presence of carbonates during the decomposition reaction [29], while nitrates arise from the mother solution. Since our synthesis procedure relies essentially on hydrolysis, carbonates are not expected and therefore, the species contained in the intersheets are supposed to be only nitrates and water molecules. Consequently, a low interlayer spacing obtained in this work could be ascribed to the small size of nitrate anions and water molecules. Vibrational studies will elucidate this aspect in the near future.

Ni 2p and O 1s XPS spectra of deposisted films on glass substrate before and after heat treatment are shown in Fig 2. NiO powder in the form of pellete was measured and used as

reference materials. The peak at 855.5 eV observed before calcination (a) is assigned to Ni $2p_{3/2}$ of $Ni(OH)_2$ [30]. Its lowering to 854.0 eV after calcining at 500 ^{o}C is indicative of the formation NiO. The associated peak at 855.5 eV is believed to be a NiO satellite peak. On the other side, 1s O peak at 531.2 eV (b) is assigned to OH$^-$ presumably derived from either $Ni(OH)_2$ or H_2O of the as-deposited film. The splitting of this 1s O peak into two components at 529.7 and 531.3 eV after heat treatment is attributed to the binding energy of NiO and OH$^-$, respectively [31].

3.2 Effect of the concentration on sample morphology

At first, the deposited films were observed with naked eyes from which, three categories of samples could be distinguished as shown in Fig.3: *(i)* samples marked with cross sign showing no deposition, *(ii)* the triangle mark referring to samples which display transparency without color, and, *(iii)* the circle mark which indicate typical thin film obtained after 24 h showing interference color. These differences were presumably caused by the reaction conditions which are related to the equilibrium factors between metal-fluoro complex and boric acid. It is suggested that the film thickness depends on the initial concentrations of dissolving species. Thereafter, the film thicknesses were evaluated by SEM measurements. In order to find out the range that favors deposition, a relationship between the morphology observed by SEM and the initial concentrations of H_3BO_3 and Ni is discussed. It can be seen from this figure that the deposition process depends upon the concentration of the treatment solution. Deposition could be observed at all range of nickel concentration examined when the concentration of boric acid is less or equal to 0.17 mol dm^{-3}. Once H_3BO_3 concentration reached 0.2 mol dm^{-3} no deposition was observed below the Ni fluoro complex concentration of 10 mmol dm^{-3}, while typical thin films were observed when it was equal to 12.5 mmol dm^{-3}. Beyond that concentration, further increase in H_3BO_3 concentration resulted in either no deposition or very thin film.

These trends are illustrated by SEM images of thin films deposited on glass substrate at various H_3BO_3 and Ni metal-fluoro complex concentrations shown in Fig. 4 and Fig. 5, respectively. Images in Fig. 4 clearly show that for a fixed concentration of nickel solution (ca.12.2 mmol dm^{-3}), the deposition process starts at H_3BO_3 concentration close to 0.2 mol dm^{-3} (a) and becomes effective at 0.1 mol dm^{-3} (b). Once the boric concentration threshold is attained, the deposition process occurs regardless how much low is the boric acid concentration. However, there is a slight change in the shape of the film's particles which exhibit two tendencies: (*i*) the width of fibers becomes larger and larger at the range of concentration between 0.075 (c) and 0.050 mmol dm^{-3} (d), with the expansion appearing with more accuracy in (d) whereas, (*ii*) the lowest concentration, 0.025 mol dm^{-3} shows fibers with similar trends as that at 0.1 mol dm^{-3}.   It can be seen from Fig. 5 that there is also a threshold concentration at ca. 6.10 $mmol/dm^3$ (b) above of which the deposition is observed. The thread-like patterns at the threshold concentration are not yet completely achieved, and large spaces are observed between them. However, from 9.15 to 18.3 mmol dm^{-3}, the deposited particles conserve a same shape, indicating that the deposition process is not greatly affected by the nickel concentration above the threshold value.

These results indicate that not only the deposition process strongly depends on H_3BO_3 concentration whereas the interference color is related to nickel concentration, but also that there is a threshold for each species above of which either the deposition process or interference color of the thin films is not significantly affected. These investigations have allowed us to set up the initial concentrations nickel and boric acid solutions at 12.5 mmol dm^{-3} and 0.1 mol dm^{-3}, respectively, in the treatment solution. Furthermore, although not shown here, SEM analyses have enabled to evaluate the thickness of samples with triangle mark to be less or equal to 180 nm while the typical thin film represented with circle has a thickness of ca. 550 nm.

The morphology and size of the particles of α-Ni(OH)$_2$ thin films obtained in this study are different from those found in the literature which are specific to each preparation procedure. For example, electron microscopy of the turbostatic nickel hydroxides in the works of Le Bihan appear as aggregates of thin crumpled sheets without any definite shape [10, 28]. Akinc et al. [12] obtained spherical agglomerates of sheet-like nanometer scale crystallites by urea decomposition. Soler-Illia et al. [9] using homogeneous alkalinization of nickel (II) nitrates by urea hydrolysis achieved petal-like shape which according to them, denotes a certain degree of unordered crystallite aggregation. Jeevanandam et al. [13] synthesized fibrous nanosheets of α-Ni(OH)$_2$ with a length of ca. 200 nm and a width of ca. 15 nm by sonochemical method while Xia and co-workers [14] obtained spherical α-phase nanocrystalline nickel hydroxide with particle sized about 20 nm by ultrasonic precipitation method. These relevant literatures confirm that the morphology and size of α-Ni(OH)$_2$ depend strongly upon the synthesis procedures.

3.3   Effect of the reaction time

The variation of the amount of Ni deposited on various substrates as a function of reaction time is shown in Fig. 6. It appears that the amount of deposited film increases almost linearly with increasing reaction time, regardless the nature of substrate, although the amount of deposited films on the alumina substrate is slightly higher than those on glass and Si wafer substrates. Their corresponding SEM images display similar features for all the three types of substrates (glass, Al$_2$O$_3$ and Si wafer) as shown in Fig. 7a. Thus, choice of substrate is governed only by the target of each experiment.

SEM images of deposited films on glass substrate (not shown) indicated that there is almost no deposition after 2 hours of reaction. The deposition process really starts after 4 hours and becomes effective after 8 hours. Further increase of the reaction time does not

affect the surface morphology of particles. This trend is corroborated by the evolution of the films thickness observed from the cross-sectional SEM images as a function of the reaction time shown in Fig. 8. The film thickness linearly increases with increasing reaction time. The analysis of the surface morphology of the deposited films at various periods of time ranging from 4 to 48 hours revealed that the film growth (which means deposition process) starts after the fourth hour and keeps going on almost proportionally with the reaction time. Cross-sectional SEM photograph showing the film thickness after 48 hours is illustrated in Fig. 9a, where ca. 1μm could be achieved.

Although the films fabricated by this process appear to have limited thickness, as we mentioned in the introduction section, relying on our previous work on β-FeOOH it is assumed that the thickness of the film can be enhanced by the solution concentration and the reaction temperature [22]. In other words, the film thickness as well as the deposition rate can be enhanced by adjusting the reaction conditions.

3.4 Effect of heat-treatment on NiO morphology

XRD patterns of NiO obtained after calcination of α-Ni(OH)$_2$ in air for an hour up to 1000°C are shown in Fig. 10. The films were deposited on Si wafer substrate after a reaction time of 48 hours. Lines appearing between 50 and 60 ^{o} obviously belong to crystalline Silicon. Reflections at 2.41, 2.08 and 1.47 Å correspond to (101), (012) and (110) planes of NiO, respectively, according to JCPDS [Card No. 22-1189] [32]. The crystalline characteristics of NiO obtained after clacination varies with temperatures. NiO peaks increase with increasing temperatures. Broaden peaks of NiO are observed up to 700 ^{o}C whereas from 800 ^{o}C, peaks become sharper and sharper. According to the XPS patterns shown in Fig.2, it seems that the formation of NiO occurs at a temperature of 500 ^{o}C after calnication of Ni(OH)$_2$.nH$_2$O by thermal decomposition. SEM images shown in Fig. 11

revealed no change in the structure of samples at the temperature up to 700°C (a) while deterioration was observed on the surface morphology from 800°C (b), and it appeared with more accuracy at 1000°C (c). It is suggested that NiO attains a metastable amorphous structure at around 500°C which stands until 700°C. Further heating to 800 ^{o}C or higher temperatures makes it become more stable. As a result, NiO diffraction peaks become sharper, indicating that a complete crystalline structure is attained. Such assumption is illustrated by cross-sectional SEM images of NiO nanoparticles after annealation at 1000°C in Fig.12a which shows highly crystallized particles. In other words, NiO structure depends on its crystallinity and, 800 ^{o}C appears to be a critical point for NiO since at this temperature, the improvement in the crystalline structure results in a deterioration of the surface morphology.

3.5 Distinction with β-Ni(OH)$_2$

Powder XRD patterns in Fig. 1b shows reflections at 4.58, 2.69, 2.32, 1.75, 1.55 and 1.46 Å which correspond to (001), (100), (011), (102), (110) and (111) planes, respectively of the typical brucite-like β-nickel hydroxides [15].

Transparent film with interference color and colorless film were deposited on the glass substrate. The obtained thin films appear as nanorods particles (see Fig. 7b) with a length of ca. 450 nm and a width of ca. 55 nm. The shapes of particles are similar with those recently reported by Wang et al. [33]. This resemblance confirms that shapes and sizes of β-Ni(OH)$_2$ also depend on the method of synthesis. The comparison of SEM images at various reaction times (not shown here) and films thickness in Fig. 8 reveals that the reaction starts and also ends earlier in the DD than in LPD method. The corollary is that thin films with a thickness of 1μm could be achieved by LPD method versus ca. 450 nm after a same reaction time of 48 hours (Fig. 9). These results suggest that direct deposition can be used as alternative

route for the synthesis of β-Ni(OH)$_2$.

It is important to mention that although the routes of synthesis used in LPD and "DD" methods are quite similar and both techniques lead to the formation of metal oxide thin films, the addition or absence of fluoride scavenger makes a big difference in their respective mechanisms. In the DD process, the formation of thin film occurs by a simple and rapid heterogeneous nucleation, and the final product may contain large amount of fluoride since no scavenger is required. Such technique has been employed by Shimizu et al. [34] for the low-temperature synthesis of anatase thin films on glass and organic substrates from aqueous solution, and by Imai et al.[35] for the preparation of anatase TiO$_2$ in porous alumina membranes. Also, the recent article by Wang et al. [33] refers to that technique where the preparation of β-nickel hydroxide could be controlled by the pH of the solution, though the authors called it "LPD". Gutiérrez-Tauste et al. have used Al(III) and Fe(III) instead of boric acid as alternative fluoride scavengers to produce TiO$_2$ films [36]. However, in the light of relevant literatures related to LPD method [17-25] including the review by Niesen [26], the deposition mechanism in the LPD process proceeds by slowly hydrolysis of an aqueous solution of a metal-fluoro complex [MF$_x^{(x-2n)-}$] by addition of water, boric acid (H$_3$BO$_3$) or aluminum metal [16,17]. The addition of water directly forces the precipitation of the oxide while boric acid or aluminum acts as fluoride scavenger which destabilizes the fluoro-complex and, forces the oxide precipitation. This step allows a much better control of the hydrolysis reaction and of the solution's supersaturation. Once the solubility limit of oxide is reached, homogeneous nucleation occur, and thin films are formed by crystal and random structured oxide layer from the substrate and the oxide layer grows onto the substrate. This justifies not only the disparity in the films thicknesses obtained after a same reaction time but also the difference in the shapes and crystalline structures of the deposited films, implying that two different synthesis procedures have been used.

The foregoing highlights that distinction should be made between the LPD and "DD" methods, and confirms so far that for the LPD method, addition of boric acid is required to destabilize the stable metal fluoro-complex bonds forcing the oxide precipitation, and at the same time to neutralize free fluoride ions in the treatment solution according to Eq. (2). It is then assumed that the remaining anions in the mother solution are adsorbed/intercalated in the interlayer space with water molecules, leading to the expansion of the c axis and as a result, the α-phase of nickel hydroxide can be formed.

4   Conclusion

The LPD method has been employed to synthesize transparent α-nickel hydroxide thin films with interference color and interconnected thread-like shapes on various substrates. The initial concentrations of nickel and boric acid solutions are crucial not only on the deposition process but also determinant for the morphology of the particles. Nanorods thin films with a length of ca. 450 nm and a width of ca. 50 nm assigned to β-Ni(OH)$_2$ could also be prepared by DD method. α-Ni(OH)$_2$ synthesized by LPD method exhibited a film thickness of ca.1μm versus 450 nm for β-Ni(OH)$_2$ prepared by DD method for the same period of time of 48 hours. The discrepancy in the crystalline structure, deposition process, shape and thickness of samples confirms that the addition of boric acid as fluoride scavenger plays an important role in the LPD process.

References

[1] N. Sac-Epée, M. R. Palacin, B. Beaudoin, A. Delahaye-Vidal, T. Jamin, Y. Chabre, T. J. Tarascon, J. Electrochem. Soc. 144 (1997) 3896.

[2] M. A. Fetcenko, S. R. Ovshinsky, B. Reichman, K. Young, C. Fierro, J. Koch, A. Zallen, W. Mays, T. Ouchi, J. Power Sources 165 (2007) 544.

[3] C. M. Lampert, Sol. Energy Mater. 19 (1989) 1.

[4] J. Nagai, G.D. McMeeking, Y. Saitoh, Solar Energy Mater. 56 (1999) 309.

[5] P. Olivia, J. Leonardi, D. Delmas, J. J. Braconnier, M. Figlarz, F. Fievret, A. de Guibert, J. Power Sources 8 (1982) 255.

[6] A. Delahaye-Vidal, M. Figlarz, J. Appl. Electrochem. 17 (1987) 589.

[7] P. V. Kamath, G. N. Subbanna, J. Appl. Electrochem. 22 (1992) 478.

[8] C. Faure, C. Delmas, P. Willmann, J. Power Sources 35 (1991) 263.

[9] G. J. A. A. Soler-Illia, M. Jobbagy, A. E. Regazzioni, M. A. Belsa, Chem. Mater 11 (1999) 3140.

[10] S. Le Bihan, M. Figlarz, J. Cryst. Growth 13-14 (1972) 458.

[11] A. Delahaye-Vidal, B. Beaudoin, N. Sca-Epee, K. Tekaia-Elhsissen, A Audemer, M. Figlarz, Solid State Ionics 84 (1996) 239.

[12] M. Akinc, N. Jongen, J. Lemaître, H. Hofmann, J. Europ. Ceram. Soc. 18 (1998) 1559.

[13] P. Jeevanandam, Y. Koltypin, A. Gedanken, Nano Lett. 1 (2001) 263.

[14] X. Xia, L. L. Shen, Z. P. Guo, H. K. Liu, G. Walter, J. Nanosci. Nanotech. 2 (2002) 45.

[15] L. X. Yang, Y. J. Zhu, H. Tong, Z. H. Liang, L. Li, L. Zhang, J. Solid State Chem. 180 (2007) 2095.

[16] H. Nagayama, H. Honda, H. Kawahara, J. Electrochem. Soc. 135 (1988) 2015.

[17] A. Hishinuma, T. Goda, M. Kitaoka, S. Hayashi, H. Kawahara, Appl. Surf. Sci. 48/49 (1991) 405.

[18] S. Deki, Y. Aoi, A. Kajinami, Chem. Lett. 16 (1996) 344.

[19] S. Deki, Y. Aoi. J. Okibe, Hiroshi Yanagimoto, A. Kajinami, M. Mizuhata, J. Mater.

Chem. 7 (1997) 1769.

[20] S. Deki, Y. Aoi, A. Kajinami, J. Mater. Sci. 32 (1997) 4269.

[21] S. Deki, Y. Aoi. H. Yanagimoto, K. Ishii, K. Akamatsu, M. Mizuhata, A. Kajinami, J. Mater. Chem. 6 (1996) 1879.

[22] S. Deki, N. Yoshida, Y. Hiroe, K. Akamatsu, M. Mizuhata, A. Kajinami, Solid Stat. Ionics 151 (2002) 1.

[23] S. Deki, S. Iizuka, A. Horie, M. Mizuhata, A. Kajinami, Chem. Lett. 25 (2004) 1747.

[24] S. Deki, H. Miki, M. Sakamoto, M. Mizuhata, Chem. Lett. 34 (2007) 518.

[25] T. P. Niesen, M. R. De Guire, Solid State Ionics 151 (2002) 61.

[26] M. Mallak, M. Bockmeyer, Peer Löbmann, Thin Solid Films 515 (2007) 8072

[27] W. Dennstedt, W. Loser, Electrochim. Acta 16 (1971) 429.

[28] S. Le Bihan, M. Figlarz, Thermochim. Acta 6 (1973) 319.

[29] F. Portemer, A. Delahaye-Vodal, M. Figlarz, J. Electrochem. Soc. 139 (1992) 671.

[30] G. B. Hoflund, W. S. Epling, Chem Mater. 10 (1998) 50.

[31] C. D. Wagner, W. M. Riggs, L. E. Davis, J. F. Moulder, G. E. Muilenberg (Editor), Handbook of X-Ray Photoelectron Spectroscopy, Perkin-Eimer, December 1978 p80.

[32] B. Post, in: W. F. McClune (Managing Editor) Power Diffraction File for Organic and Inorganic Substances, Inorganic Volume No PD1S-22iRB, Pennsylvania, 1980, p. 869.

[33] R. B. Wang, Q. Y. Li, Z. H. Wang, Q. Wei, Z. R. Nie, J. Inorg. Mater. 22 (2007) 889.

[34] K. Shimizu, H. Imai, H. Hirashima, K. Tsukuma, Thin Solid Films 351 (1999) 220.

[35] H. Imai, Y. Takei, K. Shimizu, M. Matsuda, H. Hirashima, J. Mater. Chem. 9 (1999) 2971.

[36] D. Gutiérrez-Tauste, X. Domènech, M. A. Hernàndez-Fenollosa, J. A. Aylón, J. Mater. Chem. 16 (2006) 2249.

Table 1: ICP-AES main operating parameters

Generator	1000 W
Acquisition mode	Gaussian
Nebulizer gas flow	0.51 L min^{-1}
Auxiliary gas flow	0 L min^{-1}
Plasma gas flow	12 L min^{-1}
Integration time	0.5 s
Sample flow rate	2.2 mL min^{-1}
Ni wavelength	221.647 nm

S. Deki et al. Table 1

Figure 1: XRD patterns of the deposited films on glass substrate after 48 hours: (a) α-Ni(OH)$_2$ obtained by LPD method, [Ni^{2+}]: 12.5 mmol dm^{-3}, [H$_3$BO$_3$]: 0.1 mol dm^{-3}; (b) β-Ni(OH)$_2$ obtained by DD method [Ni]: 12.5 mmol dm^{-3}, [H$_3$BO$_3$]: 0.0 mol dm^{-3}.
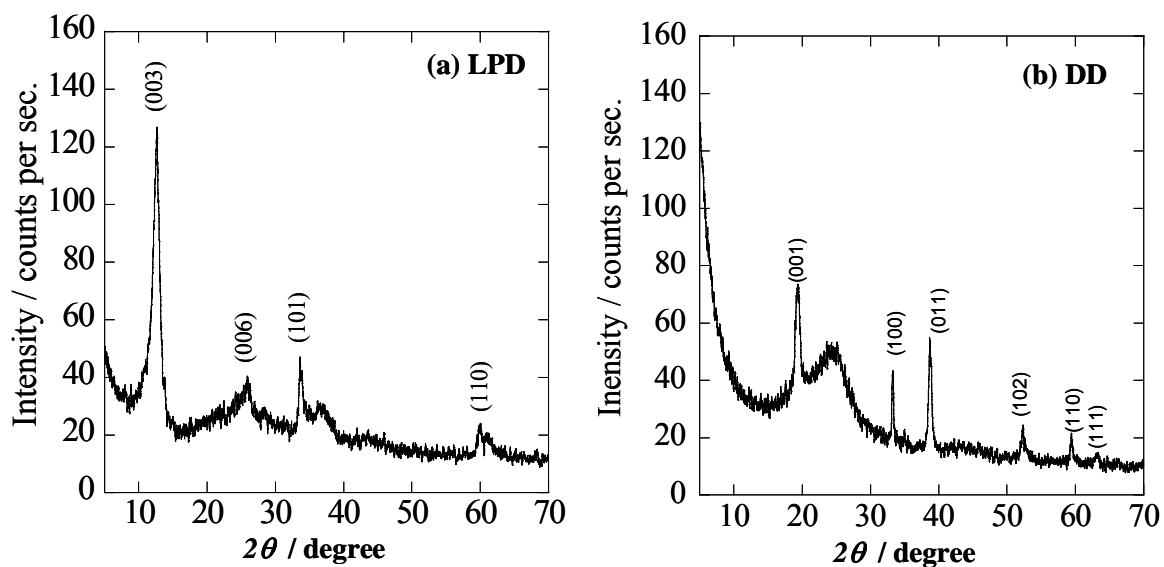
Figure 2: XPS spectra of α- Ni(OH)$_2$ thin films deposited on glass substrate after 48 hours. [Ni^{2+}]: 12.5 mmol dm^{-3}, [H$_3$BO$_3$]: 0.1 mol dm^{-3}; and NiO powders as received; (a) Ni 2p, (b) O 1s. Broken line: NiO powder as received, solid line: α-Ni(OH)$_2$ thin film as-deposited, dotted line: NiO thin film formed after annealing at 500°C.
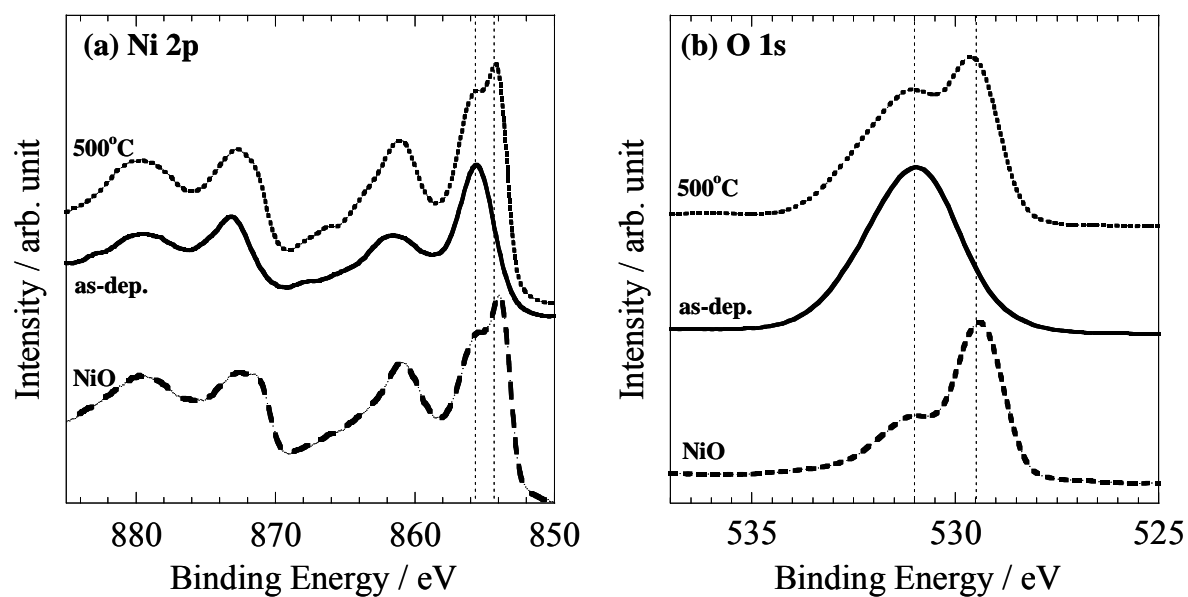
Figure 3: Relationship between the morphology of deposited films on glass substrate observed by SEM and initial concentrations of H_3BO_3 and Ni^{2+} solutions: $\bigcirc$ transparent film with interference color, $\triangle$ colorless transparent film with poor deposition, $\times$ no deposition. Reaction time: 24 hours.
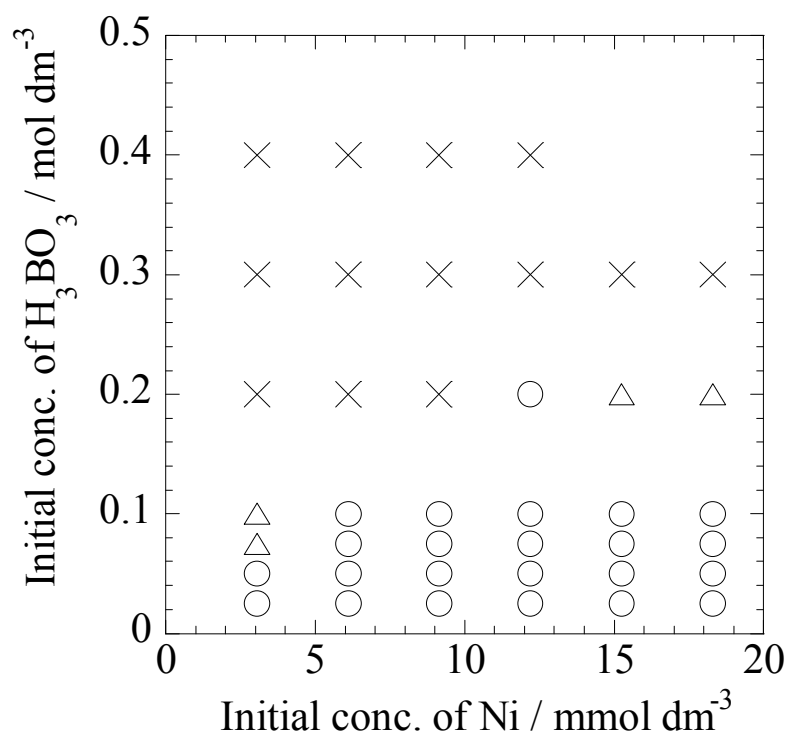
Figure 4: SEM images showing the films morphology at various H_3BO_3 concentrations for fixed Ni^{2+} concentration (12.2 mmol dm^{-3}). [H_3BO_3]: (a) 0.2 mol dm^{-3}, (b) 0.1 mol dm^{-3}, (c) 0.075 mol dm^{-3}, (d) 0.05 mol dm^{-3}, (e) 0.025 mol dm^{-3}. Reaction time : 24 h
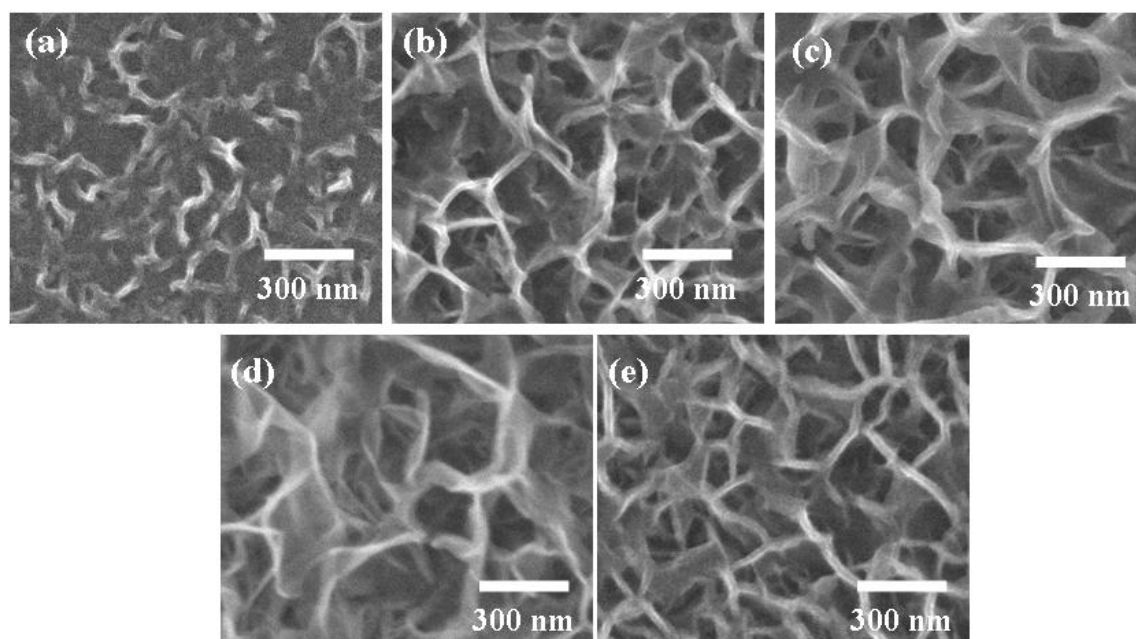
Figure 5: SEM images showing the films morphology at various Ni concentrations for fixed H_3BO_3 concentration (0.1mol dm^{-3}). [Ni^{2+}]: (a) 6.10 mmol dm^{-3}, (b) 9.15 mmol dm^{-3}, (c) 12.2 mmol dm^{-3}, (d) 15.3bmmol dm^{-3}, (e) 18.3 mmol dm^{-3}. Reaction time: 24 h.
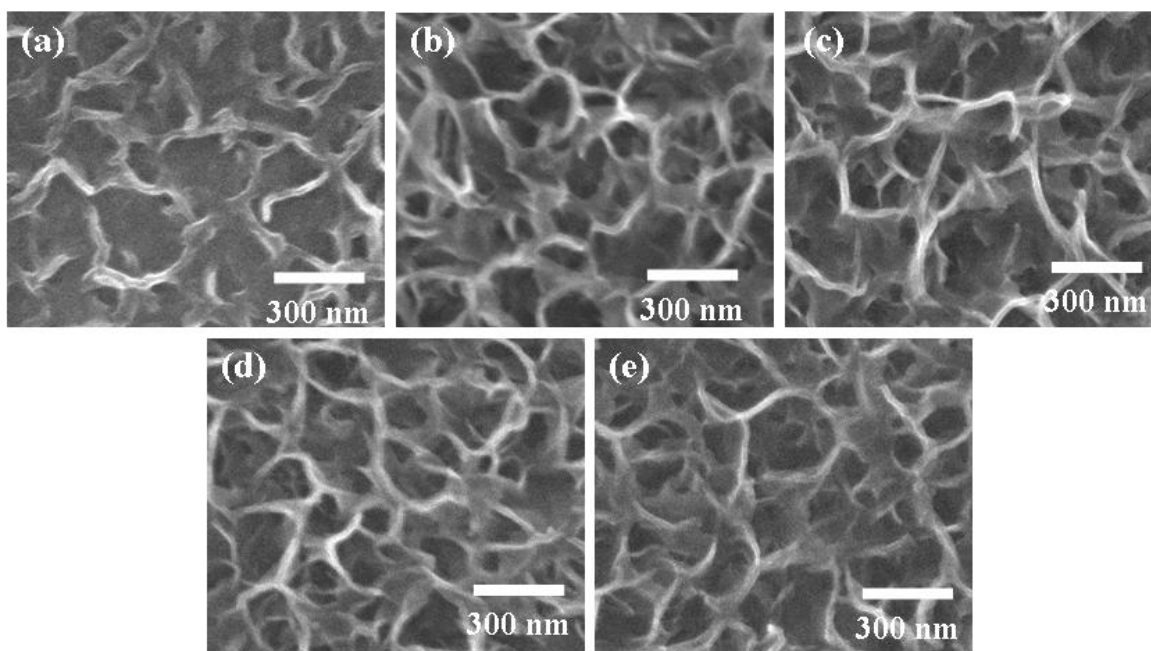
Figure 6: Variation of the Ni amount deposited on various substrates as a function of reaction time. [Ni^{2+}]: 12.5 mmol dm^{-3}, [H_3BO_3] : 0.1 mol dm^{-3}. ○ Alumina, ◆ Glass, △ Si wafer.
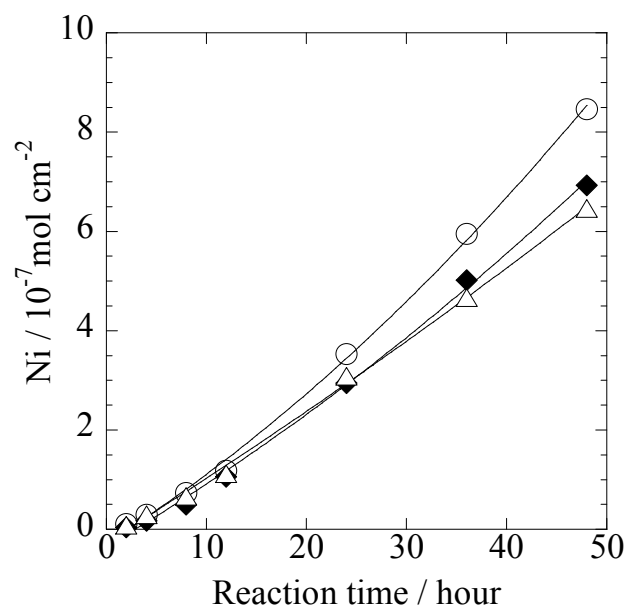
Figure 7: SEM images of deposited films on glass substrate after 48 hours: (a) α-Ni(OH)$_2$ by LPD method, [Ni^{2+}]: 12.5 mmol dm^{-3}, [H$_3$BO$_3$]: 0.1 mol dm^{-3}, (b) β-Ni(OH)$_2$ by DD method. [Ni] : 12.5 mmol dm^{-3}, [H$_3$BO$_3$] : 0.0 mol dm^{-3}.
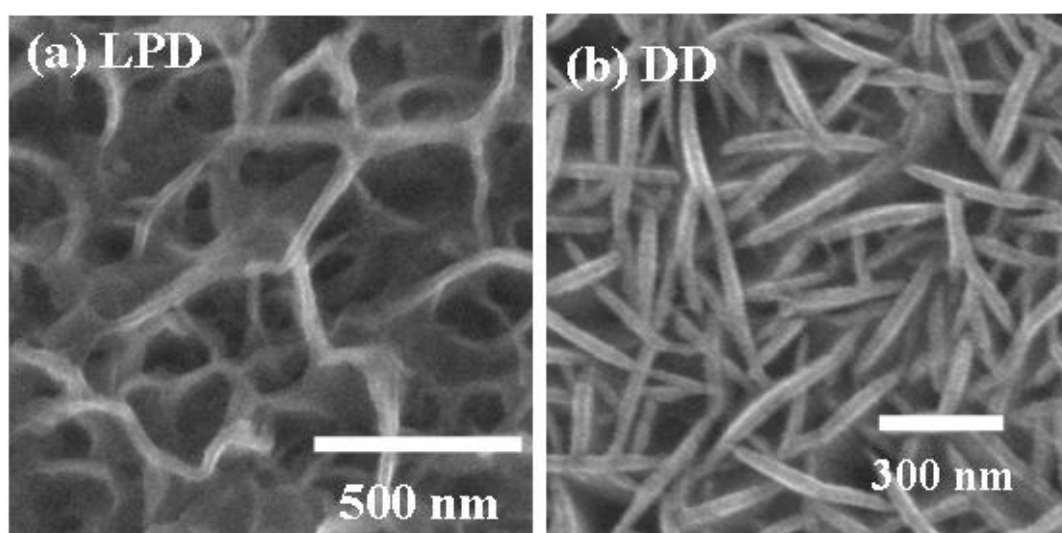

S. Deki et al. Fig. 7

Figure 8: Variation of films thickness with the reaction time. [Ni^{2+}] : 12.5 mmol dm^{-3}, ▲ 0.1 mol dm^{-3} H_3BO_3 added (LPD); △ without H_3BO_3 (DD)
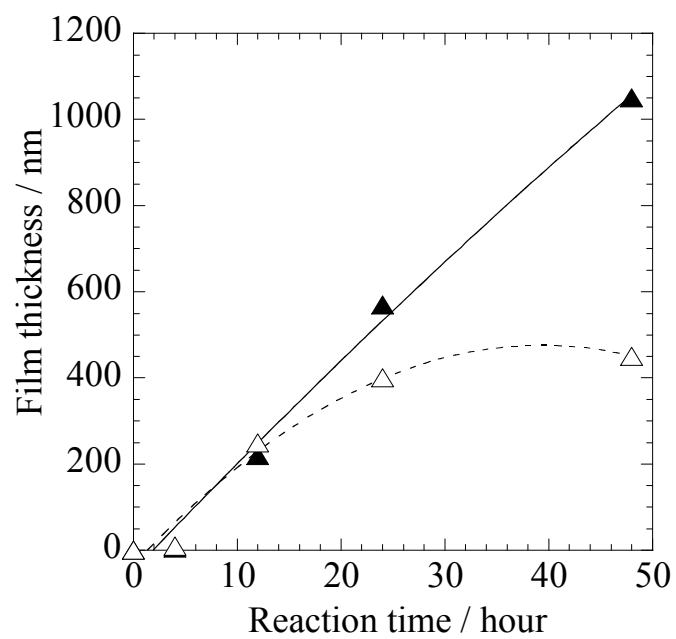
Figure 9: Cross-sectional SEM images of deposited thin films obtained after 48 hours [Ni^{2+}]: 12.5 mmol dm^{-3}, （a）0.1 mol dm^{-3} H$_3$BO$_3$ added (LPD) and, （b）without H$_3$BO$_3$ (DD)
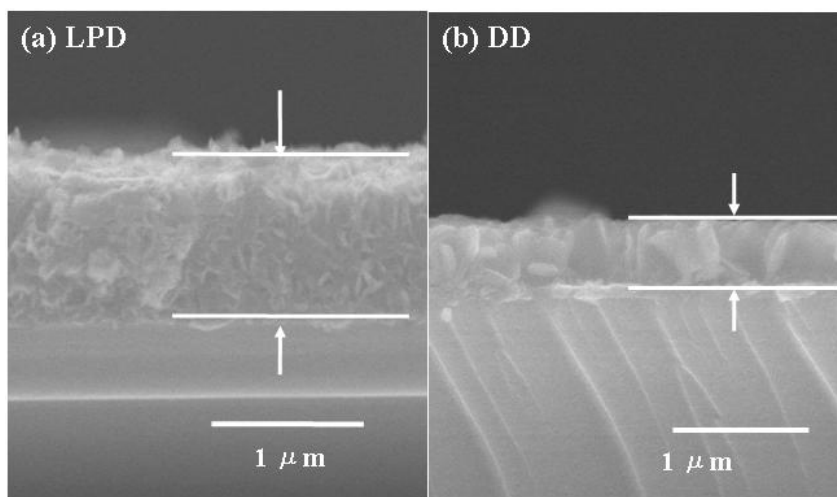
Figure 10: XRD patterns of NiO thin films formed after annealing α-Ni(OH)$_2$ in air for 1 hour at various temperatures. The films were initially deposited on Si wafer substrate for 48 h, [Ni^{2+}]: 12.5 mmol dm^{-3}, [H$_3$BO$_3$]: 0.1 mol dm^{-3}.
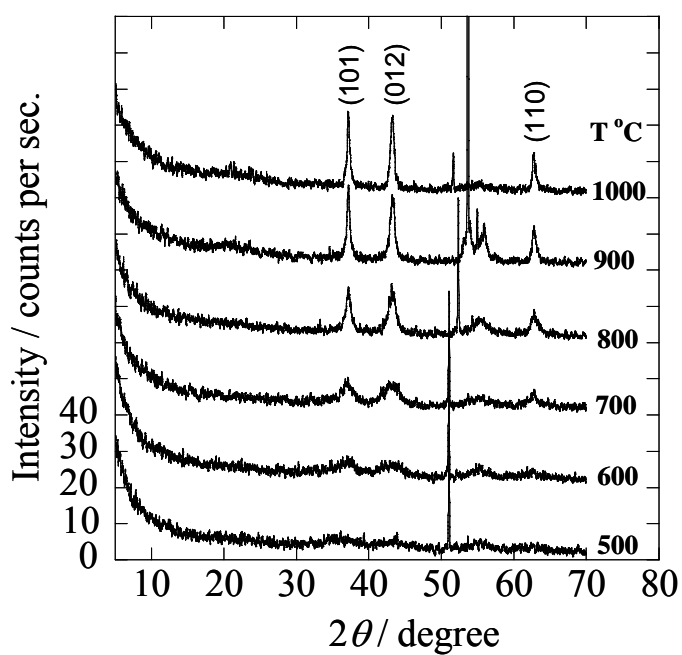
Figure 11: SEM images of NiO thin films formed after annealing α-Ni(OH)$_2$ in air for 1 hour at (a) 700°C, and (b) 800°C. The films were initially deposited on Si wafer substrate for 48 h, [Ni^{2+}]: 12.5 mmol dm^{-3}, [H$_3$BO$_3$]: 0.1 mol dm^{-3}

S. Deki et al. Fig. 11
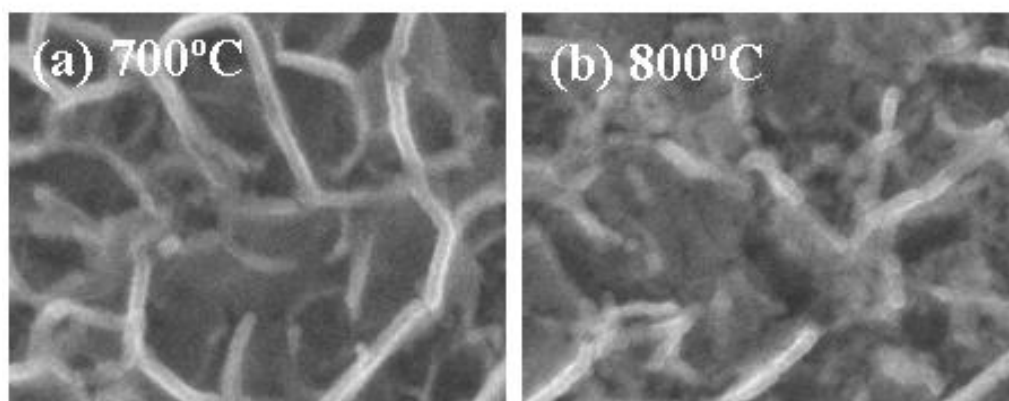
Figure 12: Cross-sectional SEM images of: (a) α-Ni(OH)$_2$ as deposited on glass substrate after 48 hours with [Ni^{2+}]: 12.5 mmol dm^{-3}, [H$_3$BO$_3$]: 0.1 mol dm^{-3}. (b) NiO obtained after annealing in air for 1 hour at 1000ºC.